Integration of Six-Phase EV Drivetrains into Battery Charging Process with Direct Grid Connection

Ivan Subotic, *Member, IEEE*, Nandor Bodo, Emil Levi, *Fellow, IEEE*

***Abstract*–The paper proposes two novel topologies for integrated battery charging of electric vehicles (EVs). The integration is functional and manifests through re-utilization of existing propulsion drivetrain components, primarily a six-phase inverter and a six-phase machine, to serve as components of a fast (three-phase) charging system. An important feature of the proposed charging systems is that they are with direct grid connection, thus non-isolated from the mains. Torque is not produced in machines during the charging process. The paper provides a comprehensive evaluation of the novel systems, together with an existing topology. Various aspects of the considered chargers are detailed and elaborated, including current balancing, interleaving modulation strategy, and influence of rotor field pulsation on control and overall performance. A control strategy is proposed and the theory and control scheme are verified by experiments.**

***Index Terms*—Battery chargers, electric vehicles, integrated on-board chargers, multiphase machines.**

I. Introduction

Various concepts for battery charging of EVs have been proposed over the years, including fast dc (off-board) charging (Fig. 1a), battery swapping, inductive (wireless) charging, conventional on-board (Fig. 1b) and integrated on-board charging (Fig. 1c) [1]. The latter is a process in which already existing power electronic components, which exist on-board an EV and that are mandatory for vehicle propulsion, are re-utilized for charging. As fewer new elements are required for the charging process, the vehicle cost, weight and required space are significantly reduced. These advantages have in the last five years put integrated chargers under extensive research focus of both academic community and industry [2].

There are two main types of integrated chargers: those that take supply from a single-phase voltage source (slow) [3] and those that are attached to three-phase mains (fast) [4]. A distinct advantage of the three-phase over the single-phase integrated chargers is a much higher charging rate. On the other hand, if a machine is integrated into three-phase charging process, three-phase currents flow through its windings, producing an undesired and harmful torque [4-5]. It causes mechanical vibrations, acoustic noise, accelerated aging of the machine, and also has a negative impact on charging efficiency. This is the main reason why most of the existing proposals relate to slow integrated chargers [6].

Manuscript received August 31, 2016; revised December 06, 2016; accepted March 02, 2017.

I. Subotic is with Power Electronic Systems Laboratory, ETH Zürich, 8092 Zürich, Switzerland (e-mail: ivansubotic86@gmail.com).

N. Bodo is with the Bristol Blue Green, Liverpool L7 9NJ, UK (e-mail: nbodo@bristolbluegreen.com)

E. Levi is with the Faculty of Engineering and Technology, Liverpool John Moores University, Liverpool L3 3AF, UK (e-mail: e.levi@ljmu.ac.uk).

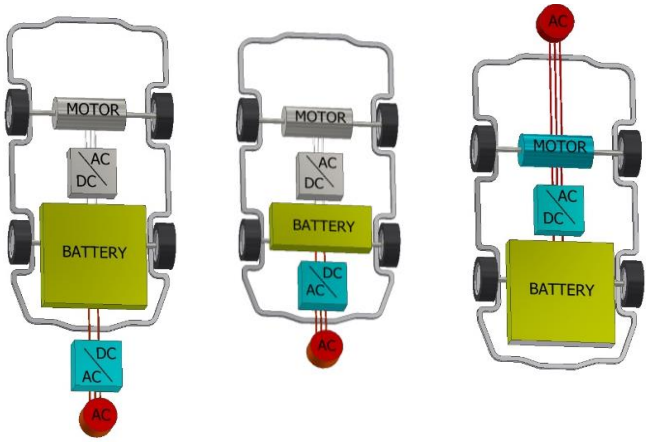

Fig. 1. Conductive battery charging types: a) off-board, b) non-integrated on-board, c) integrated on-board.

There were several attempts to avoid torque production during fast integrated charging process [7-11]. These include utilization of a synchronous machine with an excitation winding that can be disconnected during the charging process [7], utilization of a non-integrated rectifier in front of the machine [8-9], drivetrains with multiple machines [10], and a machine with accessible mid-points of windings [11] (an equivalent of a symmetrical six-phase machine). However, when it comes to a standard three-phase induction (IM) and permanent-magnet (PM) machine, which can be found in most of EVs [12], there does not seem to be a straightforward manner to avoid torque production without introducing additional non-integrated hardware elements.

However, if multiphase machines are considered for integration, the situation changes dramatically. Unlike three-phase machines, they possess current components that are not capable of torque production. In [13-14] it is shown how these current components can be utilized for torque-free charging process using nine- and five-phase machines, respectively. However, machines with six phases are still the most frequently utilized multiphase machines and their integration into the charging process is considered in [4, 15]. However, solution in [15] requires an off-board line-frequency transformer on the grid side, which significantly increases the charging infrastructure cost, while in [4] there is a torque production in a machine which is utilized as a transformer.

This paper introduces two novel six-phase integrated charging topologies that do not have the above mentioned shortcomings. They are based on utilization of a machine with double three-phase windings (two three-phase windings spatially in phase) and a symmetrical six-phase machine. They are considered together with an existing topology from [16], based on utilization of an asymmetrical six-phase machine.

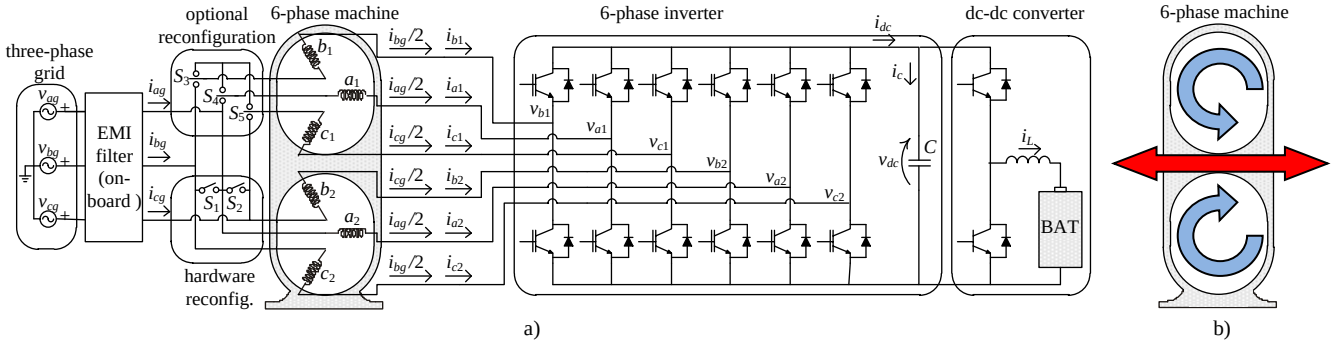

Fig. 2. a) A general scheme of the proposed six-phase charging topologies. The figure is represented for the case of employment of the machine with dual stator windings, b) Representation of flux production in the machine during the charging process, given for the topology employing the machine from Fig. 2a.

The topologies have distinct advantages over all previously proposed solutions [13-15]. Unlike [14], two machine phases conduct each grid current, allowing the topologies to achieve a charging/propulsion power ratio of 100% compared to 60% in [14]. In contrast to [15], they do not need a transformer, since they do not require a multiphase set of voltages, which leads to cost saving. As a three-phase rather than multiphase voltage supply is utilized, the control differs considerably. Effect of a pulsating field in the rotor (which was only mentioned in passing in [15]) and balancing current control (which was not considered at all in [15]) are comprehensively analysed. Finally, compared to [13] the same is achieved with a smaller number of phases as each set of windings produces a rotating field, and the cancellation is performed at the level of the whole machine rather than at the level of each set separately, as in [13]. As a result, they offer the cheapest integration with a charging power reaching propulsion power.

The paper is organised as follows. The topologies are presented in Section II. Section III provides evaluation of torque production during the charging process. A comprehensive analysis of influence of rotor field on equivalent charging scheme is given in Section IV. Section V discusses control in charging and vehicle-to-grid (V2G) mode, while Section VI provides comprehensive current control algorithms. Experimental results are given in Section VII, while Section VIII concludes the paper.

II. Charging Topologies

A general scheme of all three considered topologies is depicted in Fig. 2a. Although the machine has a single stator and rotor, in Fig. 2 the two sets of three phases are depicted separately for clearer view. If there is no spatial shift between the two three-phase sets (phases a_1 and a_2), like in Fig. 2a, the machine corresponds to a three-phase machine with double stator windings. When the spatial shift is 30 degrees the six-phase machine is called asymmetrical [16], while the shift of 60 degrees makes the machine symmetrical. The similarity of the machine without a spatial shift between the two three-phase sets to a standard three-phase machine allows utilization of traditional machine design and control knowledge in this type of six-phase machine. The other two machines are obtainable by stator rewinding of a three-phase machine.

Hardware reconfiguration is required between the propulsion and the charging/V2G mode, and it is accomplished by contactors S_1-S_2 and S_3-S_5 (if required). In propulsion mode contactors S_1 and S_2 are closed, while contactors S_3-S_5 are in the upper position. This yields the machine topology with two isolated neutral points. At this point it should be noted that if the machine is operated with a single neutral point in propulsion, contactors S_3-S_5 are in both charging/V2G and propulsion mode in the lower position, so they are not required. In this case only contactors S_1-S_2 are sufficient to perform hardware reconfiguration. Control of all three machine types in propulsion mode is well-known regardless of the number of isolated neutral points, and it is therefore not considered in this paper.

In charging/V2G mode contactors S_1 and S_2 are opened and S_3-S_5 are in the lower position. This connects grid phases *ag*, *bg* and *cg* to machine phases a_1, b_1 and c_1, respectively. However, it at the same time connects grid phases to phases of the second set with a modified phase order. Namely, the grid phases are connected to phases a_2, c_2 and b_2 respectively. Inverter/rectifier legs connected to the same grid phase are controlled with the same modulation signals.

The modified order of connections achieves that the stator field that is produced by the second set has the opposite direction of rotation from the field that is produced by the first set (Fig. 2b), when three-phase currents flow from/to the grid. The accomplishment is that the resulting stator field pulsates along a single direction (Fig. 2b). As a pulsating field is not capable of producing a starting torque, the machine does not have to be mechanically locked during the charging process. Theoretical assessment of torque production in all three charging topologies is considered in the next section.

It should be noted that the industrial standard for EV battery chargers is the existence of an EMI (electro-magnetic interference) filter towards the grid. However, the majority of the proposed integrated chargers are without the EMI filter as it would interfere with the propulsion mode. In all the proposed topologies in this paper, the EMI filter exists on-board the vehicle (Fig. 2a). Its interference with the propulsion mode is prevented by contactors S_1 and S_2, which are the only mandatory non-integrated elements for all topologies. The contactors significantly differ from switches that are required in converters (IGBTs and MOSFETs), both by functionality and cost. The contactors do not introduce operational losses as they are only used to change the mode of operation, from charging/V2G mode to propulsion and vice versa.

III. Evaluation of Torque Production

Machine torque production evaluation is of paramount importance for integrated charging, since it should be avoided.

However, its existence cannot be assessed by means of speed measurement. Namely, if a machine that is not locked does not rotate during the charging/V2G process, it does not imply that it is not producing a very harmful torque. A torque can still be present, although incapable of surpassing friction. A convenient and reliable manner of gathering precise information on torque existence is observation of machine currents in a decoupled domain. In what follows, this method is elaborated and employed to assess torque production in the three discussed topologies.

Decoupling matrices of six-phase systems differ from the one for systems with three phases. Three-phase systems have three currents, of which only two are independent (i.e., can have any value), and the third phase current can be obtained from the first two (if there is no zero-sequence current). Therefore, there are only two degrees of freedom. However, the two actual currents are not orthogonal; thus a decoupling matrix has to be introduced. It keeps the number of degrees of freedom the same, while making the current components mutually orthogonal.

On the other hand, six-phase systems have six phase currents, of which four or five are independent (i.e., can have any value) depending on whether there are two isolated or a single neutral point, respectively. Therefore, there are four or five degrees of freedom. Again, the currents are not mutually orthogonal. For that reason a decoupling matrix is introduced. It again keeps the number of degrees of freedom the same, but makes the components mutually orthogonal. As the result, the first two components (α and β components) are responsible for field and torque production in the machine, while the remaining components (x, y, 0_+ and 0_-) are responsible for losses. Finally, each component pair can be represented in a single two-dimensional plane whose axis are the two corresponding orthogonal components.

For symmetrical six-phase systems decoupling matrix can be obtained from its general multiphase form given in [17], while for the asymmetrical system it is given in [16]. Decoupling matrix of dual three-phase systems is governed with [18]:

$$\underline{C} = \frac{1}{\sqrt{3}} \begin{bmatrix} 1 & \cos\left(\frac{2\pi}{3}\right) & \cos\left(\frac{4\pi}{3}\right) & 1 & \cos\left(\frac{2\pi}{3}\right) & \cos\left(\frac{4\pi}{3}\right) \\ 0 & \sin\left(\frac{2\pi}{3}\right) & \sin\left(\frac{4\pi}{3}\right) & 0 & \sin\left(\frac{2\pi}{3}\right) & \sin\left(\frac{4\pi}{3}\right) \\ 1 & \cos\left(\frac{4\pi}{3}\right) & \cos\left(\frac{2\pi}{3}\right) & -1 & \cos\left(\frac{\pi}{3}\right) & \cos\left(\frac{5\pi}{3}\right) \\ 0 & \sin\left(\frac{4\pi}{3}\right) & \sin\left(\frac{2\pi}{3}\right) & 0 & \sin\left(\frac{\pi}{3}\right) & \sin\left(\frac{5\pi}{3}\right) \\ 1 & 1 & 1 & 0 & 0 & 0 \\ 0 & 0 & 0 & 1 & 1 & 1 \end{bmatrix} \tag{1}$$

Grid standards and regulations demand that all currents taken from or injected into the grid have to be sinusoidal and in phase or phase opposition with grid phase voltages. Hence, currents that are taken from the grid have to be governed with:

$$i_{kg} = \sqrt{2} I \cos(\omega t - l 2\pi/3) \quad k = a,b,c \quad l = 0,1,2 \tag{2}$$

Pure observation of Fig. 2a is sufficient to determine the correlations between machine and grid currents as:

$$i_{a1} = i_{a2} = \frac{i_{ag}}{2}; \quad i_{b1} = i_{c2} = \frac{i_{bg}}{2}; \quad i_{c1} = i_{b2} = \frac{i_{cg}}{2} \tag{3}$$

which is valid for all three topologies. The machines' behaviour is uniquely determined by currents flowing through

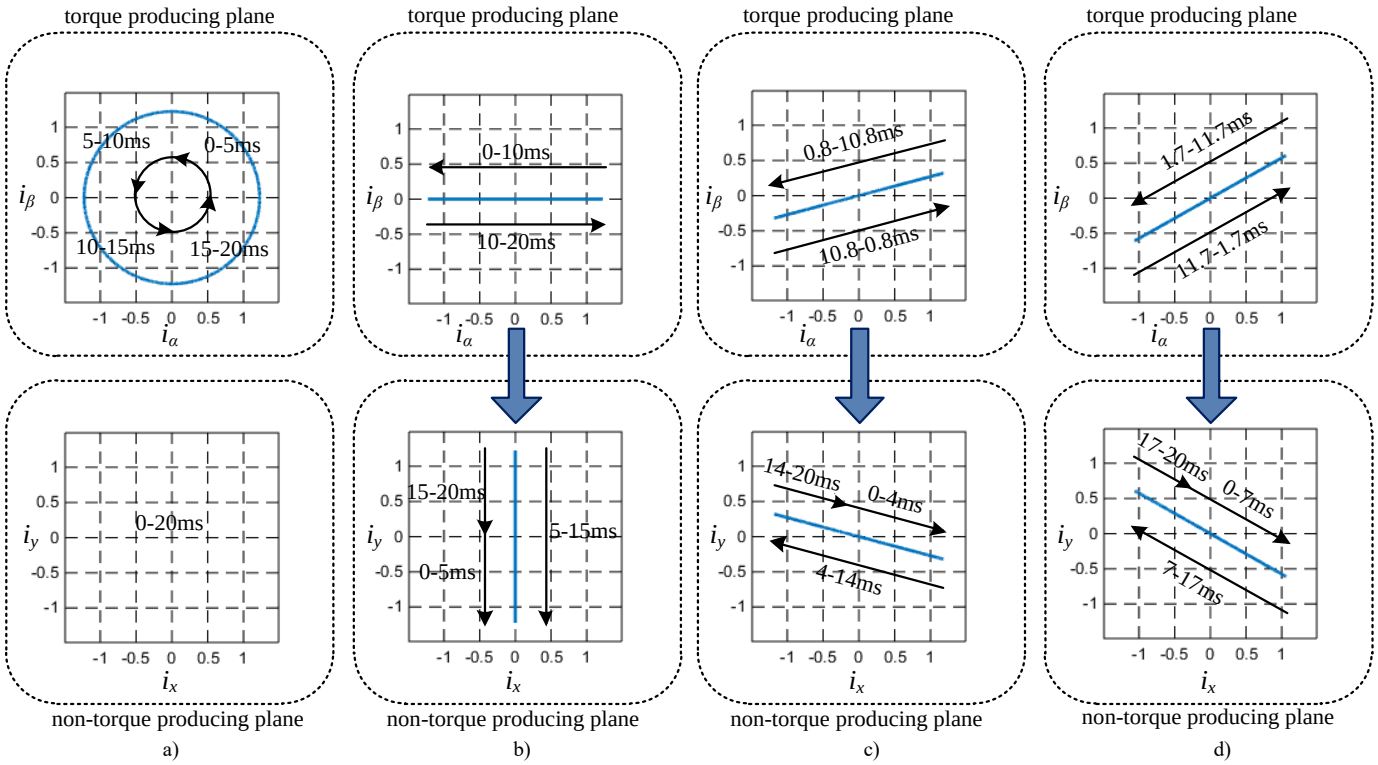

Fig. 3. Graphical representation of theoretical results given in Table I. The excitation mapping into the machines' planes is given for: a) propulsion mode of all three machines, and charging mode (50Hz) of the b) dual stator winding machine, c) asymmetrical six-phase machine, d) symmetrical six-phase machine.

TABLE I: MAPPING OF EXCITATION INTO MACHINES' PLANES

Topology	Excitation in torque producing plane	Excitation in non-torque producing (passive) plane
Double three-phase	$\underline{i}_{\alpha\beta} = \sqrt{\frac{3}{2}} \cdot I \cdot \cos(\omega t)$	$\underline{i}_{xy} = \sqrt{\frac{3}{2}} \cdot I \cdot \cos(\omega t + \pi/2)$
Asymmetrical 6 phase	$\underline{i}_{\alpha\beta} = (1.18 + j \cdot 0.32) \cdot I \cdot \cos(\omega t - \pi/12)$	$\underline{i}_{xy} = (0.32 + j \cdot 1.18) \cdot I \cdot \cos(\omega t + 5\pi/12)$
Symmetrical 6-phase	$\underline{i}_{\alpha\beta} = (1.06 + j \cdot 0.61) \cdot I \cdot \cos(\omega t - \pi/6)$	$\underline{i}_{xy} = (0.61 + j \cdot 1.06) \cdot I \cdot \cos(\omega t + \pi/3)$

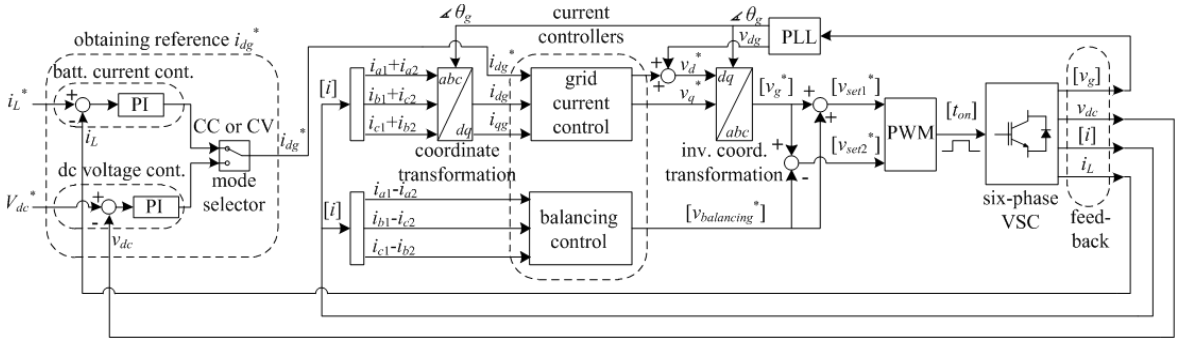

Fig. 5. The main control algorithm for the battery charging mode of operation.

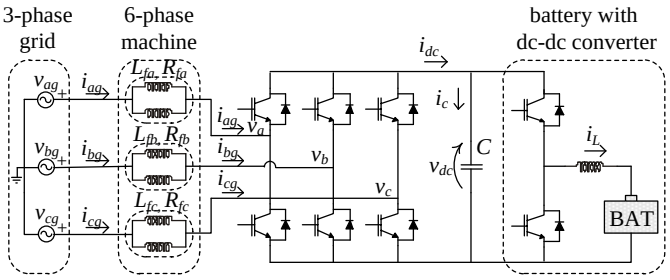

Fig. 4. Equivalent scheme of the topologies from Fig. 2.

them (2)-(3). In order to assess torque production these currents are transformed into a decoupled domain. For the double three-phase topology this is achieved by substituting (2) into (3); (3) is further formulated as a 6x1 column matrix of phase currents and then transformed with (1). For the other two topologies, instead of (1), the corresponding decoupling transformation matrices [16-17] are used. The results are given in Table I. The derivations are given in Appendix A.

As six-phase systems are being transformed, the decoupled systems have six components each, three more than systems with three-phases. From Table I it can be seen that excitation utilizes four of these components. These are *α-β* components which exist in three-phase systems and are in charge of torque/flux production, and additional two components denoted with *x-y*, which are incapable of producing a torque. Table I implies that a significant amount of excitation is transferred from the *α-β* into *x-y* components. If *α-β* components are represented in the *α-β* plane, this transfer achieves that only a pulsating excitation remains in the *α-β* plane. The pulsating excitation produces a pulsating field in the stator which is incapable of producing a starting torque.

Expressions given in Table I are verified utilizing Matlab and graphically depicted in Fig. 3 in order to facilitate the analysis. Obviously, unlike in the propulsion mode, a part of the excitation is indeed transferred from the first (torque-producing) into a second (non-torque producing) plane, leaving only a pulsating excitation in both planes. It can be concluded that in the all three topologies there is no torque production during charging/V2G process.

IV. INFLUENCE OF ROTOR FIELD PRODUCTION ON THE CHARGING MODE EQUIVALENT SCHEME

In the previous section it is shown that in all three topologies there is no torque production in the machines during the charging/V2G process. Thus, in these modes the machines can be represented as a simple set of passive components, namely *R-L* elements (Fig. 4). As pairs of two converter legs are operated with the same modulation signals, in this mode representation as a three-phase power factor correction (PFC) converter (Fig. 4) can be used. Inverter legs, shown in Fig. 2, which are connected (through the machine) to the same grid phase, are represented with a single leg in Fig. 4. The equivalent circuit allows bidirectional operation (charging and V2G) and is valid for all three discussed topologies.

However, the previous section clearly shows that all topologies feature a production of a pulsating field in the stator (Table I), which in turn produces an induced pulsating field in the rotor. This rotor field interferes with the per-phase equivalent filter values. As the rotor is stationary the machine can be observed as a three-phase transformer with short circuited secondary windings (and a small air gap). Such transformer has equivalent scheme consisting of the sum of primary and secondary leakage inductances and resistances. Therefore, in the machines the rotor leakage inductance and resistance will increase the values of filter per-phase impedances. This is beneficial as the increase in filter impedances lowers the grid current ripple.

However, the influence of the rotor pulsating field is not the same among the machine phases. Spatially, the field appears in a single direction. Therefore, its highest impact is on the machine phases that are on the direct axis of pulsation, or its immediate vicinity. These phases experience the highest increase in their equivalent filter impedance. On the other hand, it does not influence phases that are shifted by 90° from this direction (e.g. in the symmetrical six-phase topology,

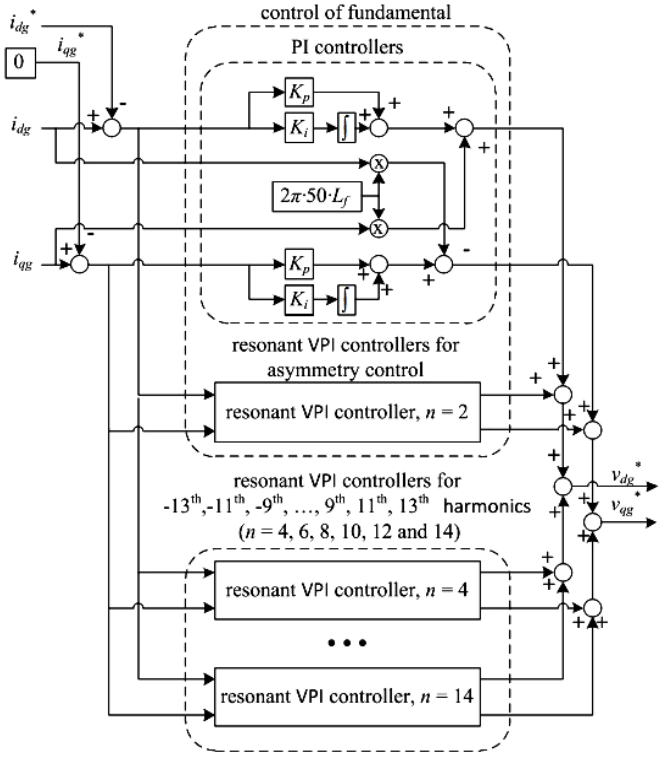

Fig. 6. "Grid current control" block from Fig 5.

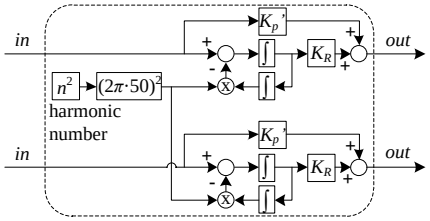

Fig. 7. "Resonant VPI controller" block from Fig. 6.

phases b_1 and c_2 are at the right angle from the axis of field pulsation). These phases do not experience any increase in per-phase filter impedance caused by the rotor. Therefore, machine phases in the vicinity of the direction of field pulsation (in all three topologies these are the phases a_1 and a_2) have higher equivalent per-phase filter impedance than other phases, which introduces asymmetry in the system. As a result, the circuit of Fig. 4 differs from the standard three-phase PFC boost converter by having different values of per-phase filter impedances in different phases ($R_{fa} \neq R_{fb} \neq R_{fc}$ in Fig. 4). However, the effect of parameter imbalance can be completely supressed by appropriate current control, described in Section VI.

V. Control in Constant-Current and Constant-Voltage Modes

Grid standards and regulations demand that the charging process takes place at unity power factor. In order to ensure this, the voltage-oriented control (VOC) is commonly used. Its control algorithm is well-known and it is utilized in many applications, as well as in the majority of proposed integrated chargers. However, topologies proposed here require a modified version of VOC, which is depicted in Fig. 5.

The process initiates with measurements of grid voltages, dc-bus voltage, machine currents and battery charging current (which is equal to dc-bus current if dc-dc converter is not utilized). Grid currents do not require separate measurement sensors, since they can be completely reproduced from machine currents by employing (3).

From the grid voltages, information on grid voltage vector angle can be obtained by means of phase-locked loop (PLL). The information is utilized to transform grid currents into a reference frame that rotates at the same speed and aligns with the grid voltage vector. This is done in the "coordinate transformation" block in Fig. 5, which contains both decoupling and rotational transformation. The rotating transformation is beneficial as in this reference frame grid currents are seen as two dc components - one in phase with the voltage vector (i_{dg}) and another shifted by 90° from it (i_{qg}). Achieving unity power factor now becomes straightforward. It only requires controlling the current component that is in phase with the voltage vector (i_{dg} component) to its reference and keeping the other current component (i_{qg}) at zero.

A standard manner of obtaining the current reference for the charging process is by the constant current – constant voltage (CC-CV) strategy. The process initiates with the CC mode, where the reference for the battery charging current is set to a constant and maximal allowed value. This regime terminates when the battery voltage reaches certain "cut-off" level. Beyond that point the battery is charged by a constant voltage (Fig. 5). The current in this mode slowly decreases and the process lasts until the current drops to 10% of its maximum value, which represents the end of the charging process.

When battery charging current reference is obtained (either from CC or CV mode) it is employed to control grid current components in the block "grid current control", which is separately discussed in the next section. From the output of the "grid current control" block, converter reference voltages can be easily obtained by applying "inverse coordinate transformation" – Fig. 5.

In order to have the same currents in converter phases that are connected to the same grid phase, it is not sufficient to control them with the same modulation signals since it is rarely the case that two machine phases have completely identical parameters. Small differences in parameters can cause harmful currents that circulate among machine phases without entering the grid, causing increased heating and deteriorated efficiency. Moreover, they are capable of causing undesired torque production in the machine. These harmful currents are controlled to zero in the block "balancing control", separately discussed in Section VI.

Finally, converter reference values enter the PWM block, which utilizes a standard carrier-based modulation strategy with interleaving and with zero-sequence injection. It should be noted that the control algorithm of Fig. 5 is applicable for both charging and V2G mode of operation.

VI. Current Control

Current control blocks from Fig. 5 are shown in detail in Figs. 6-8 and are discussed in what follows.

A. Fundamental Grid Current Control

Current components i_{dg} and i_{qg} are dc quantities. Thus, they

can be easily controlled to their references (i_{dg}^* and 0, respectively) with PI controllers shown in Fig. 6. This is sufficient for control of current fundamental in symmetrical systems (where $R_{fa} = R_{fb} = R_{fc}$). However, as already noted in Section IV, filter per-phase parameters are not the same ($R_{fa} \neq R_{fb} \neq R_{fc}$), thus the system is not symmetrical. This results in a current component that rotates at synchronous speed in anti-synchronous direction (observed from the stationary reference frame). This current component appears as the second harmonic in the synchronous reference frame. It can be completely zeroed by a pair of resonant vector proportional integral (VPI) current controllers tuned at the second harmonic – Fig. 6. The scheme of a resonant VPI current controller of Fig. 6 is depicted in Fig. 7.

Parameters of the current controllers have been determined by "modulus optimum" method, based on the closed loop model of the system.

B. Harmonic Compensation

Inverter dead-time is the main source of harmonics in the system. These are primarily –5th, 7th, –11th and 13th (as seen from the stationary reference frame). From the synchronous reference frame, these harmonics are seen as -6^{th}, 6^{th}, -12^{th} and 12^{th}. They can conveniently be zeroed by two pairs of resonant VPI current controllers tuned at 6th and 12th harmonic. This is sufficient for a proper control of symmetrical systems and gives satisfactory results for systems where parameter asymmetry is not high. However, in systems with a pronounced parameter asymmetry (such as those in this paper) it cannot completely zero the harmonics. Namely, in asymmetrical systems harmonics also have additional components that rotate in the opposite direction than in symmetrical systems. Thus, although with very small values, the 5^{th}, -7^{th}, 11^{th} and -13^{th} (as seen from the stationary reference frame) harmonics are introduced. From the synchronous reference frame these harmonics are seen as the 4^{th}, -8^{th}, 10^{th} and -14^{th}. Therefore, the corresponding resonant VPI current controllers have to be added to the system. The scheme shown in Fig. 6 is capable of complete removal of harmonics, as will be verified in Section VII.

C. Current Balancing

Differences between each two machine phase currents connected to the same grid phase are fed into block "balancing control", which is shown separately in Fig. 8. As already noted these current components are harmful and can even cause torque production in the machine. They can be zeroed in the stationary reference frame by three resonant VPI controllers, as shown in Fig. 8, and verified in Section VII-F.

D. Modulation Strategy with Interleaving

An advantage of the proposed topologies is that the modulation strategy with interleaving can be employed in order to decrease grid current switching ripple and facilitate compliance with grid standards and regulations. Interleaving consists of phase shifting of the carriers of the machine phases that are connected to a common branch and have the same modulation signal. The shift between the carriers is equal to 360° divided by the number of phases sharing the common

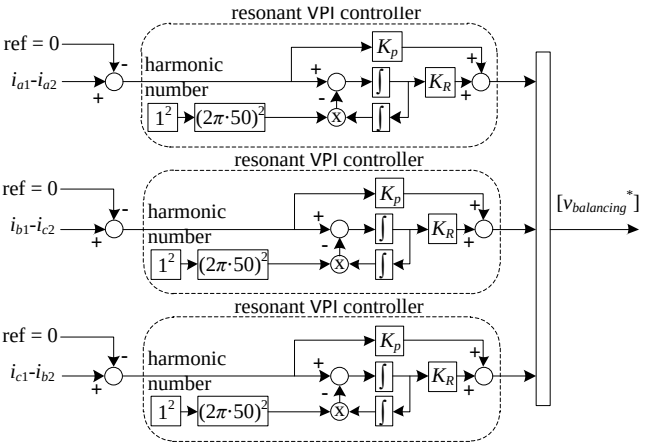

Fig. 8. "Balancing control" block from Fig. 5.

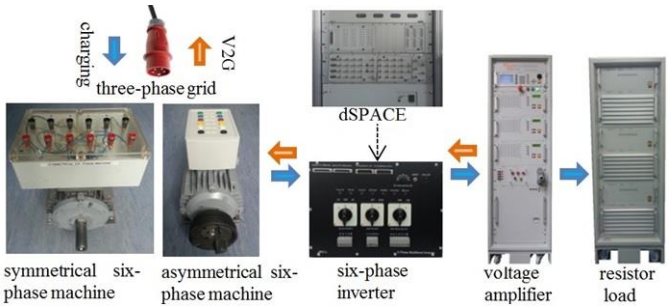

Fig. 9. Experimental rig.

branch. In the proposed topologies pairs of two phases share the common branch, thus the phase shift is 180 degrees. The influence of interleaving process on overall performance is evaluated in Sections VII-G.

VII. Experimental Results

In order to evaluate viability of the proposed topologies and to validate the theoretical discussions and developed control, experiments are performed with the symmetrical and asymmetrical topology. The topologies are operated in both charging and V2G mode. The integrated chargers take/inject power directly from/to a three-phase grid, 415V, 50Hz. A linear amplifier "Spitzenberger & Spies" is used to emulate the battery and a dc-dc converter (whose absence or presence in the topology is governed by the battery voltage and the grid voltage levels). It produces at the output a voltage that is equal to the high voltage side of the dc-dc converter (i.e. dc-bus voltage). Thus a dc-dc converter is not used. The utilized six-phase converter (whose scheme is shown in Fig. 2 and is labelled "six-phase inverter") has a dead time of 6μs and operates at 10kHz, with asymmetrical PWM. Thus the control executes at 20kHz. In the symmetrical topology small external inductances are attached to machine phases in order to effectively increase its leakage inductances (which are very low for the particular machine – see Appendix B). Experimental rig is depicted in Fig. 9, while the rig data are provided in Appendix B.

A. Charging Mode

The charging mode is demonstrated for the symmetrical six-phase topology (Fig. 10) and it is performed at i_{dg}^*=2A. All

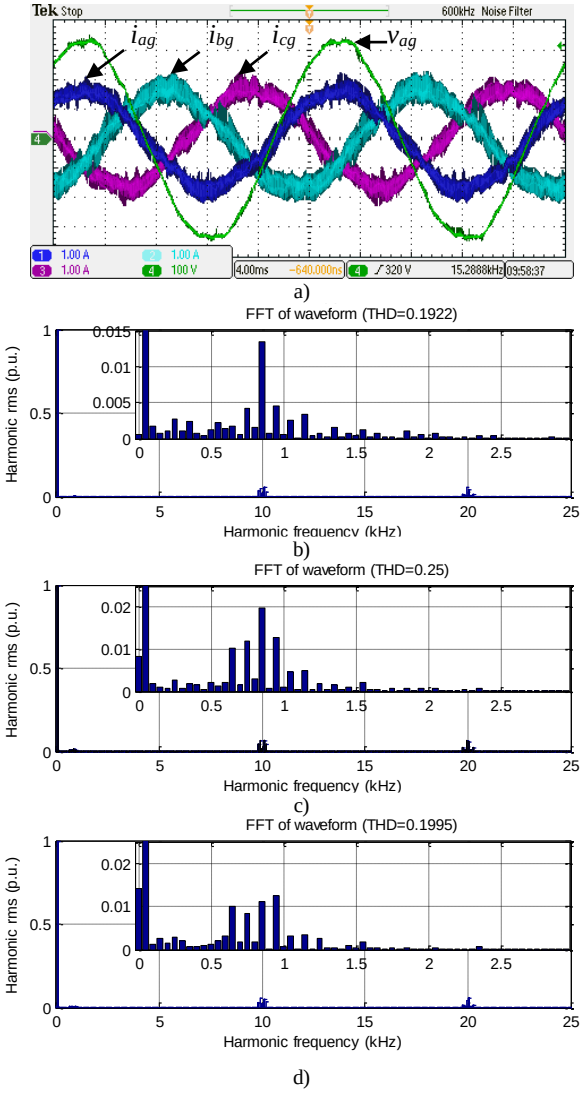

Fig. 10. Charging mode of operation of the topology employing a symmetrical six-phase machine: a) grid phase voltage v_{ag}, and grid currents i_{ag}, i_{bg} and i_{cg}, b-d) spectra of grid currents i_{ag}, i_{bg} and i_{cg}, respectively.

three grid currents together with grid phase voltage are shown in Fig. 10a. It can be seen that the currents are in phase with grid voltages, achieving unity power factor. It is interesting to note that the phase "*a*" has the smallest current ripple. This is in accordance with the theory in Section IV, which states that the rotor pulsating flux affects the most phases a_1 and a_2, and increases their equivalent impedances. These two phases are both attached to the grid phase "*ag*" (3), leading to the smallest current ripple in this phase. However, although the parameter imbalance is obvious, all three currents have the same rms values (1.16A, 1.17A and 1.16A), which validates the proposed control given in Section VI-A.

B. V2G Mode

V2G mode of operation is demonstrated for the asymmetrical six-phase topology (Fig. 11) and is performed at i_{dg}^{*}= -1A. Fig. 11a depicts grid phase voltage v_{ag}, machine currents i_{a1} and i_{a2}, and battery charging current i_L (which of course has a negative value). Again, unity power factor operation is obvious. The two machine phase currents have rms values of 0.305A and 0.295A, which demonstrates that

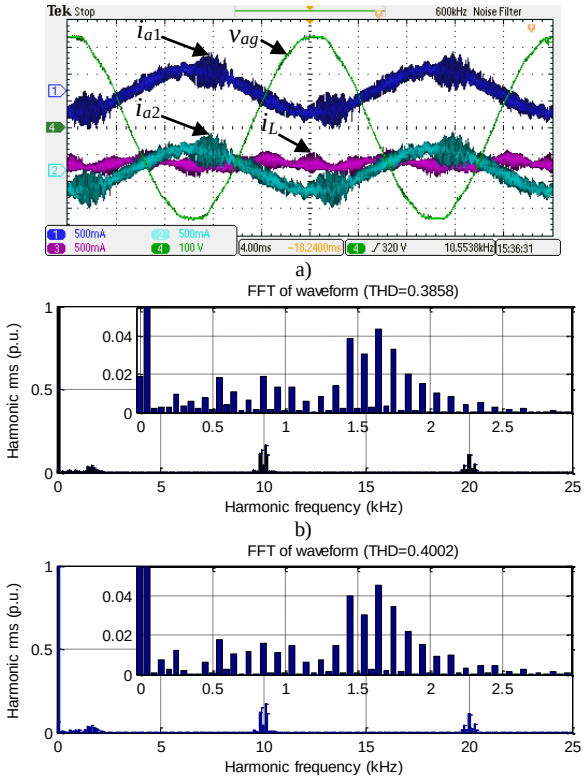

Fig. 11. V2G mode of operation of the asymmetrical six-phase topology: a) grid phase voltage v_{ag}, and machine currents i_{a1} and i_{a2}, b-c) spectra of machine currents i_{a1} and i_{a2}, respectively.

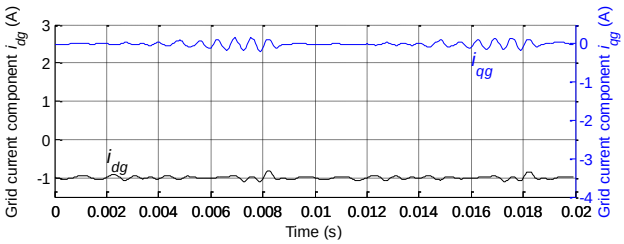

Fig. 12. Grid current components i_{dg} and i_{qg} during the V2G operation of the topology with the asymmetrical six-phase machine.

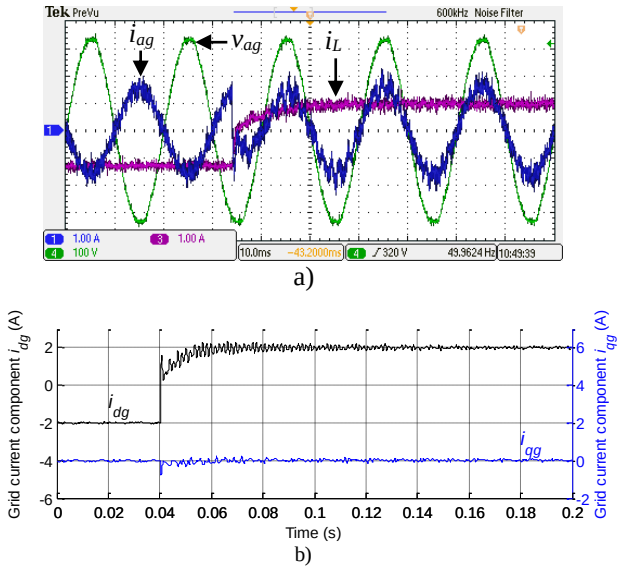

Fig. 13. Transient from V2G into charging mode of operation given for the topology employing the symmetrical six-phase machine: a) grid phase voltage, grid current and battery charging current, b) grid current components.

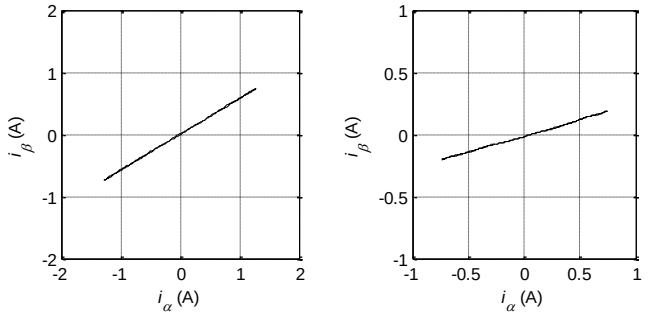

Fig. 14. Excitation in the first (torque-producing) plane during the charging mode employing the symmetrical (left) and the asymmetrical machine (right).

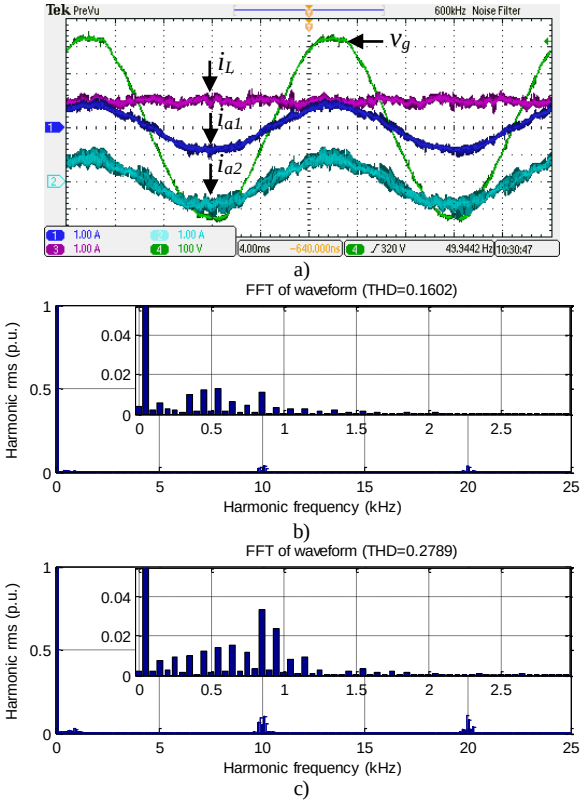

Fig. 15. Demonstration of current balancing among machine phases when one external inductance is removed from the symmetrical topology in charging mode of operation: a) grid phase voltage v_{ag}, machine currents i_{a1} and i_{a2}, and battery charging current i_L, b-c) spectrums of machine currents i_{a1} and i_{a2}.

grid current i_{ag} is properly balanced between them. Grid current components are shown in Fig. 12. The *d*-component tracks its reference well, while the *q*- component is controlled to zero, which again verifies unity power factor operation.

C. Transient

In order to demonstrate transient performance, the transfer from V2G into charging mode is performed. It is shown in Fig. 13 for the case of the symmetrical topology. From Fig. 13a it can be seen that the system features high dynamic capabilities. Fig. 13b shows that while *d* current component is utilized for energy transfer, the *q* component is kept at zero, ensuring unity power operation during the whole transient.

D. Torque Production Assessment

During all experiments the speed was measured by resolvers, which gave zero speed reading at all times. However, this is not sufficient to claim zero torque production and hence machine current components have to be observed. They are shown in Fig. 14 for the charging mode of both asymmetrical and symmetrical topology. As can be seen, the excitation in the torque producing (α-β) plane is along a single direction in both cases. This results in an appearance of a pulsating field, which is not capable of producing any starting torque. Experimental results are in accordance with the theoretical results of Section III (Fig. 3).

E. Harmonic Compensation

Without the control of the grid current low order harmonics, it is noted that the grid current has such harmonics that rotate in both synchronous and anti-synchronous direction. This is in accordance with the theory of symmetrical components, as the system has pronounced parameter asymmetry between the grid phases. In experiments it is confirmed that the low order harmonics cannot be completely supressed until additional controllers (Fig. 6) for harmonics rotating in the anti-synchronous direction are introduced (Section VI). Figures 10b-d and 11b-c show that in both observed systems low order harmonics have very low values (below 2%).

F. Current Balancing

Each grid phase is attached to two machine phases which share its current. If impedances of the two phases are the same, they can be hard-paralleled to share the grid current equally. However, real systems always exhibit small mismatch between the impedances of any two phases, leading to unequal sharing of the grid current, which may cause severe problems (Section V). In Fig. 11 the ability of control to supress the small parameter differences and equally share the grid current among the two phases has already been demonstrated. However, in order to exacerbate the problem and fully test the control abilities, an external inductance is removed from one machine phase (phase a_2) of the symmetrical topology, while the other phases retained their external inductances.

Experimental results of the grid current i_{ag} sharing among the phases a_1 and a_2 of the machine are demonstrated in Fig. 15. From Fig. 15a it is obvious that current switching ripple is significantly higher in the phase without the external inductance (a_2), which can also be seen from its THD (Fig. 15c). Nevertheless, the control achieves very similar rms values of both currents (0.58A and 0.60A). Thus equal sharing of the grid current i_{ag} is accomplished despite the high parameter asymmetry. It can be concluded that both parameter asymmetry and inevitable parameter variations during the operation are easily suppressed by the control.

G. Modulation Strategy with Interleaving

The effect of the application of the interleaving in the modulation is demonstrated in the case of the symmetrical topology. The results are shown in Fig. 16. It can be seen that the charging is again with unity power factor, and that grid currents again have very small values of low order harmonics. However, if compared with Fig. 10, it can be seen that the grid current switching ripple is significantly reduced. The reason is that a part of the current switching harmonics gets closed within the machine itself without entering the grid. On the other hand, this increases the losses in the machine and is not

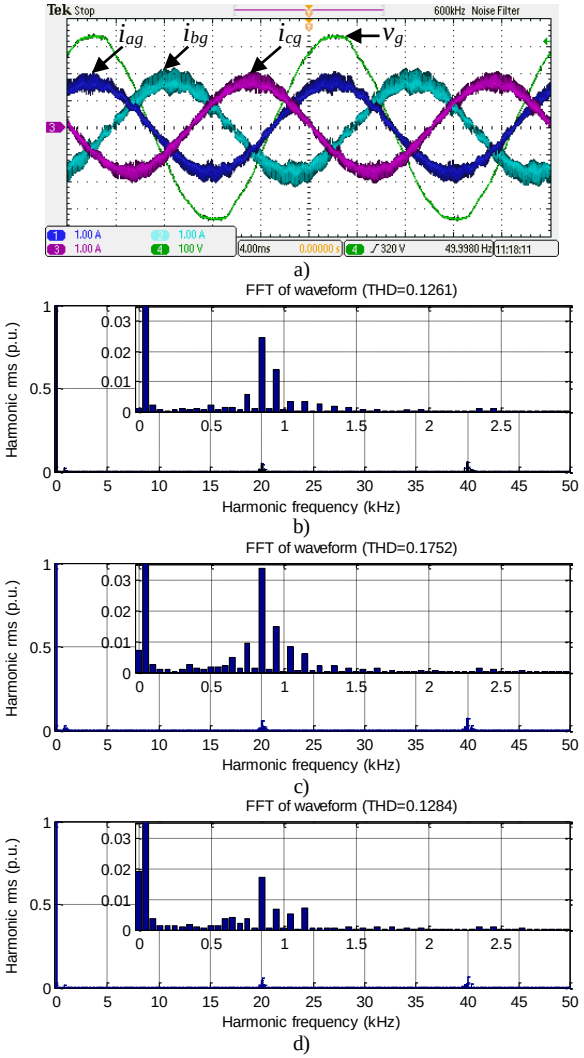

Fig. 16. The symmetrical six-phase topology in charging mode of operation employing interleaving modulation strategy: a) grid phase voltage v_{ag} and currents i_{ag}, i_{bg} and i_{cg}, b) spectrums of grid currents i_{ag}, i_{bg}, i_{cg}, respectively.

always justified (especially in systems with very low values of filter inductance), as demonstrated in [19].

VIII. Conclusion

The paper introduces novel charging topologies that integrate six-phase machines into charging process with direct grid connection. The topologies do not require a line-frequency transformer at the front, which allows substantial cost savings. Influence of a pulsating field production in all the topologies is analysed, and it is demonstrated that a torque is not produced during the charging/V2G operation. A control capable of fully supressing the parameter asymmetry, which is introduced by the pulsating field, as well as supressing parameter unbalance between machine phases is proposed. A comprehensive experimental investigation has been conducted and the results fully support theoretical developments.

Appendix A

Derivation procedure for all equations in Table I is similar. Therefore, only a general illustration is provided here for the case of the symmetrical six-phase topology.

Decoupling real Clarke's matrix for the symmetrical six-phase machines can be found in [17]. It is beneficial to represent it in a space vector form:

$$\underline{i}_{\alpha\beta} = i_\alpha + j i_\beta = \sqrt{2/6}\left(i_{a1} + \underline{a} i_{a2} + \underline{a}^2 i_{b1} + \underline{a}^3 i_{b2} + \underline{a}^4 i_{c1} + \underline{a}^5 i_{c2}\right) \tag{4}$$

$$\underline{i}_{xy} = i_x + j i_y = \sqrt{2/6}\left(i_{a1} + \underline{a}^2 i_{a2} + \underline{a}^4 i_{b1} + \underline{a}^6 i_{b2} + \underline{a}^8 i_{c1} + \underline{a}^{10} i_{c2}\right) \tag{5}$$

where $\underline{a} = \exp(j\delta) = \cos\delta + j\sin\delta$ and $\delta = 2\pi/6$.

Grid currents are given with (2), while the correlation between machine and grid currents is governed with (3). Substitution of (2) and (3) into (4) leads to the following expression:

$$\begin{aligned}\underline{i}_{\alpha\beta} = \sqrt{\frac{2}{6}} \cdot I \cdot \frac{\sqrt{2}}{2} \Bigg\{ & \frac{1}{2}\left(e^{j\omega t} + e^{-j\omega t}\right)\left(1 + e^{j\delta}\right) + \\ & + \frac{1}{2}\left(e^{j(\omega t - \frac{2\pi}{3})} + e^{-j(\omega t - \frac{2\pi}{3})}\right)\left(e^{j2\delta} + e^{j5\delta}\right) + \\ & + \frac{1}{2}\left(e^{j(\omega t - \frac{4\pi}{3})} + e^{-j(\omega t - \frac{4\pi}{3})}\right)\left(e^{j3\delta} + e^{j4\delta}\right)\Bigg\}\end{aligned} \tag{6}$$

Components that are multiplied by $e^{j\omega t}$ and those multiplied by $e^{-j\omega t}$ can be separated, after which the following expressions are obtained:

$$\begin{aligned}\underline{i}_{\alpha\beta} = \frac{I}{2\sqrt{6}} \Bigg\{ & e^{j\omega t} \cdot \left[\left(1 + e^{j\delta}\right) + e^{-j\frac{2\pi}{3}}\left(e^{j2\delta} + e^{j5\delta}\right) + e^{-j\frac{4\pi}{3}}\left(e^{j3\delta} + e^{j4\delta}\right)\right] + \\ & + e^{-j\omega t} \cdot \left[\left(1 + e^{j\delta}\right) + e^{j\frac{2\pi}{3}}\left(e^{j2\delta} + e^{j5\delta}\right) + e^{j\frac{4\pi}{3}}\left(e^{j3\delta} + e^{j4\delta}\right)\right]\Bigg\}\end{aligned} \tag{7}$$

$$\underline{i}_{\alpha\beta} = \frac{I}{2\sqrt{6}}\left[e^{j\omega t} \cdot (3 - j \cdot 0) + e^{-j\omega t} \cdot (1.5 + j \cdot 2.598)\right] \tag{8}$$

$$\underline{i}_{\alpha\beta} = \frac{I}{2\sqrt{6}}\left[e^{j\omega t} \cdot 3 \cdot e^{j0} + e^{-j\omega t} \cdot 3 \cdot e^{j(\frac{\pi}{3})}\right] \tag{9}$$

$$\underline{i}_{\alpha\beta} = \frac{I}{2\sqrt{6}} \cdot 3 \cdot e^{j(\frac{\pi}{6})}\left[e^{j\omega t} \cdot e^{-j(\frac{\pi}{6})} + e^{-j\omega t} \cdot 3 \cdot e^{j(\frac{\pi}{6})}\right] \tag{10}$$

$$\underline{i}_{\alpha\beta} = \frac{I}{2\sqrt{6}} \cdot 3 \cdot e^{j(\frac{\pi}{6})}\left[e^{j(\omega t - \frac{\pi}{6})} + e^{-j(\omega t - \frac{\pi}{6})}\right] \tag{11}$$

$$\underline{i}_{\alpha\beta} = \frac{I}{\sqrt{6}} \cdot 3 \cdot e^{j(\frac{\pi}{6})} \cdot \cos\left(\omega t - \frac{\pi}{6}\right) \tag{12}$$

$$\underline{i}_{\alpha\beta} = (1.06 + j \cdot 0.61) \cdot I \cdot \cos\left(\omega t - \frac{\pi}{6}\right) \tag{13}$$

The result clearly represents the expression given in Table I for the symmetrical six-phase system. The excitation in the second (*x-y* plane) can be obtained in the same manner; the same applies for the remaining two topologies.

Appendix B: Experimental Rig Data

Symmetrical six-phase induction machine: the parameters are $R_s = 3.6\Omega$, $R_r = 1.8\ \Omega$, $L_m = 205$mH, $L_{ys} = 8.1$mH, $L_{yr} = 11.5$mH. The machine has three pole pairs, 50 Hz, 110 V (phase-to-neutral), 1.1kW, 900 rpm.

Asymmetrical six-phase induction machine: the parameters are R_s = 12.5Ω, R_r = 6Ω, L_m = 590mH, $L_{\gamma s}$ = 61.5mH, $L_{\gamma r}$ = 11mH. A six-pole machine is obtained by rewinding a 380 V, 50 Hz, 1.1 kW three-phase machine.

Small external inductances: 10mH per grid phase. They are utilized only with the symmetrical six-phase topology.

Dc source/sink: "Spitzenberger & Spies" – two DM 2500/PAS systems connected in series. Power sinking up to 4kW is enabled by an additional resistive load RL 4000, which is shown in Fig. 9 and is labelled as "resistor load".

Controller: dSPACE DS1006 processor board. DS2004 high-speed A/D board and DS5101 Digital Waveform Output Board are used for the A/D conversion of measured signals and PWM signal generation. Incremental Encoder Interface Board DS3002 is used to validate that machines do not move during the charging/V2G process.

Converter: Custom made eight-phase inverter with EUPEC FS50R12KE3 IGBTs. Using the heat-sink data, it is estimated that the rated continuous output rms current is 14A, which gives for a 240V rms phase voltage for six phases of inverter continuous rating of approximately 20kVA.

REFERENCES

[1] D.G. Woo, D.M. Joo, and B.K. Lee, "On the feasibility of integrated battery charger utilizing traction motor and inverter in plug-in hybrid electric vehicles," *IEEE Trans. on Power Electronics*, vol. 30, no. 12, pp. 7270-7281, 2015.

[2] N. Sakr, D. Sadarnac and A. Gascher, "A review of on-board integrated chargers for electric vehicles," *Proc. Eur. Conf. on Power Electronics and Applications EPE-ECCE*, Lappeenranta, Finland, 2014.

[3] I. Subotic and E. Levi, "A review of single-phase on-board integrated battery charging topologies for electric vehicles," *IEEE Workshop on Electrical Machines Design, Control and Diagnosis WEMDCD*, Torino, Italy, pp. 136-145, 2015.

[4] S. Haghbin, S. Lundmark, M. Alakula, and O. Carlson, "Grid-connected integrated battery chargers in vehicle applications: review and new solution," *IEEE Trans. on Industrial Electronics*, vol. 60, no. 2, pp. 459-473, 2013.

[5] X. Lu, K.L.V. Iyer, K. Mukherjee, and N.C. Kar, "Investigation of integrated charging and discharging incorporating interior permanent magnet machine with damper bars for electric vehicles," *IEEE Trans. on Energy Conversion*, vol. 31, no. 1, pp. 260-269, 2016.

[6] M. Yilmaz and P.T. Krein, "Review of integrated charging methods for plug-in electric and hybrid vehicles," *Proc. IEEE Int. Conf. on Vehicular Electronics and Safety ICVES*, Istanbul, Turkey, 2012.

[7] P. Dupuy, "Electric traction chain for an automobile," *US Patent No. US 2011/0187185 A1*, 2011.

[8] S. Loudot, B. Briane, O. Ploix, and A. Villeneuve, "Fast charging device for an electric vehicle," *US Patent No.* US 8,847,555 B2, 2014.

[9] J. Hong, H. Lee, and K. Nam, "Charging method for the secondary battery in dual-inverter drive systems for electric vehicles," *IEEE Trans. on Power Electronics*, vol. 30, no. 2, pp. 909-921, 2015.

[10] G. J. Su, "Electric vehicle system for charging and supplying electrical power," *US Patent No. US 7,733,039 B2*, 2010.

[11] L. De Sousa and B. Bouchez, "Combined electric device for powering and charging," *US patent No. US 2011/0221363 A1*, 2011.

[12] J. D. Santiago, H. Bernhoff, B. Ekergård, S. Eriksson, S. Ferhatovic, R. Waters, and M. Leijon, "Electrical motor drivelines in commercial all-electric vehicles: A review," *IEEE Trans. on Vehicular Technology*, vol. 61, no. 2, pp. 475-484, 2012.

[13] I. Subotic, N. Bodo, E. Levi, and M. Jones, "On-board integrated battery charger for EVs using an asymmetrical nine-phase machine," *IEEE Trans. on Industrial Electronics*, vol. 62, no. 5, pp. 3285-3295, 2015.

[14] I. Subotic, N. Bodo, and E. Levi, "An EV drive-train with integrated fast charging capability," *IEEE Trans. on Power Electronics*, vol. 31, no. 2, pp. 1461-1471, 2016.

[15] I. Subotic, N. Bodo, E. Levi, M. Jones, and V. Levi, "Isolated chargers for EVs incorporating six-phase machines," *IEEE Trans. on Industrial Electronics*, vol. 63, no. 1, pp. 653-664, 2016.

[16] I. Subotic, E. Levi and N. Bodo, "A fast on-board integrated battery charger for EVs using an asymmetrical six-phase machine," *Proc. Vehicle Power and Propulsion Conf. VPPC*, Coimbra, Portugal, 2014.

[17] E. Levi, R. Bojoi, F. Profumo, H.A. Toliyat, and S. Williamson, "Multiphase induction motor drives - a technology status review," *IET Electric Power Applications*, vol. 1, no. 4, pp. 489-516, 2007.

[18] D. Hadiouche, H. Razik and A. Rezzoug, "Modelling of a double-star induction motor with an arbitrary shift angle between its three phase windings," *Int. Conf. on Power Electronics and Motion Control EPE-PEMC*, Kosice, Slovakia, 2000.

[19] N. Bodo, E. Levi, I. Subotic, J. Espina, L. Empringham, M. Johnson, "Efficiency evaluation of fully integrated on-board EV battery chargers with nine-phase machines," *IEEE Trans. on Energy Conversion*, vol. 32, no. 1, pp. 257-266, 2017.

Ivan Subotic (S'12, M'16) received the Dipl. Ing. and MSc degrees in Electrical Engineering from the University of Belgrade, Belgrade, Serbia, in 2010 and 2011, respectively. He has been with the Liverpool John Moores University, Liverpool, U.K., as a PhD student since 2011. He received his PhD degree in September 2015 and is now with the ETH Zurich, as a post-doctoral research associate. His main research interests include power electronics, electric vehicles, and control of multiphase drive systems.

Nandor Bodo received his Masters degree in 2009 in Power Electronics from the University of Novi Sad, Faculty of Technical Sciences, Novi Sad, Serbia and his PhD degree in Electrical Engineering in 2013 from Liverpool John Moores University, Liverpool, UK. From September 2013 until March 2016 he was with the Liverpool John Moores University, Liverpool, UK as a post-doctoral research associate. He is now with the Bristol Blue Green, Liverpool, UK.

Emil Levi (S'89, M'92, SM'99, F'09) received his MSc and the PhD degrees in Electrical Engineering from the University of Belgrade, Yugoslavia in 1986 and 1990, respectively. He joined Liverpool John Moores University, UK in May 1992 and is since September 2000 Professor of Electric Machines and Drives. He served as a Co-Editor-in-Chief of the IEEE Trans. on Industrial Electronics in the 2009-2013 period and is currently Editor-in-Chief of the IET Electric Power Applications and an Editor of the IEEE Trans. on Energy Conversion. He is the recipient of the Cyril Veinott award of the IEEE Power and Energy Society for 2009 and the Best Paper award of the IEEE Trans. on Industrial Electronics for 2008. In 2014 he received the "Outstanding Achievement Award" from the European Power Electronics (EPE) Association.